Available online at www.sciencedirect.com
ScienceDirect
Polymer 47 (2006) 8495–8508
polymer
www.elsevier.com/locate/polymer

Influence of the oxidation state of phosphorus on the decomposition and fire behaviour of flame-retarded epoxy resin composites

Ulrike Braun [a], Aliaksandr I. Balabanovich [a], Bernhard Schartel [a,*], Uta Knoll [a], Johannes Artner [b], Michael Ciesielski [b], Manfred Döring [b], Raul Perez [c], Jan K.W. Sandler [c], Volker Altstädt [c], Thorsten Hoffmann [d], Doris Pospiech [d]

[a] *Federal Institute for Materials Research and Testing, Unter den Eichen 87, 12205 Berlin, Germany*
[b] *Research Centre Karlsruhe GmbH, Institute of Technical Chemistry, 76021 Karlsruhe, Germany*
[c] *Polymer Engineering, University of Bayreuth, Universitätsstraße 30, 95440 Bayreuth, Germany*
[d] *Leibniz-Institute of Polymer Research Dresden, Hohe Straße 6, 01069 Dresden, Germany*

Received 23 August 2006; received in revised form 11 October 2006; accepted 19 October 2006
Available online 13 November 2006

Abstract

A systematic and comparative evaluation of the pyrolysis of halogen-free flame-retarded epoxy resins containing phosphine oxide, phosphinate, phosphonate, and phosphate (phosphorus contents around 2.6 wt.%) and the fire behaviour of their carbon fibre composites is presented. Decomposition pathways are proposed based on the thermal analysis (TG), TG coupled with evolved gas analysis (TG-FTIR), kinetics and analysis of the residue with FTIR and XPS. All organophosphorus-modified hardeners containing phenoxy groups lead to a reduced decomposition temperature and mass loss step for the main decomposition of the cured epoxy resin. With increasing oxidation state of the phosphorus the thermally stable residue increases, whereas the release of phosphorus-containing volatiles decreases. The flammability of the composites was investigated with LOI and UL 94 and the fire behaviour for forced-flaming conditions with cone calorimeter tests performed using different irradiations. The flame retardancy mechanisms are discussed. With increasing oxidation state of the phosphorus additional charring is observed, whereas the flame inhibition, which plays the more important role for the performance of the composites, decreases. The processing and the mechanical performance (delamination resistance, flexural properties and interlaminar bonding strength) of the fibre-reinforced composites containing phosphorus were maintained at a high level and, in some cases, even improved. The potential for optimising flame retardancy while maintaining mechanical properties is highlighted in this study.

Keywords: Fire retardant; Composites; Organophosphorus-containing epoxy resin

1. Introduction

Composites offer advantages over metals such as lower weight, improved fatigue performance, and no corrosion, such that they are increasingly used in the transportation sector. The manufacture of large parts for both general aviation and commercial aircrafts has become an important force driving the development of ever-improving carbon fibre-reinforced epoxy resins. Composites are to make up a large share of the structural weight of new aircraft: over 20% of the new Airbus A 380, and more than 50% of the new Boeing 787. In the case of the latter aircraft even the fuselage and wings will be constructed of composite materials. Assuming that the aircraft producers will be forced to demonstrate that the polymer composite structures provide safety equivalent to the current material systems, there is a demand for research and development of novel flame-retarded fibre-reinforced epoxy resin. The challenge entails achieving the property profile defined by the

* Corresponding author. Tel.: +49 30 8104 1021; fax: +49 30 8104 1027.
E-mail address: bernhard.schartel@bam.de (B. Schartel).

0032-3861/$ - see front matter © 2006 Elsevier Ltd. All rights reserved.
doi:10.1016/j.polymer.2006.10.022

production technologies, high-performance mechanical properties and effective flame retardation.

The use of phosphorus-containing compounds as promising, halogen-free, either reactive or additive flame retardants for epoxy resins has been discussed extensively and reviewed [1–3]. It becomes clear that reactively flame-retarded epoxy resins not only enable feasibility in principle, but also have the potential for practical applications in halogen-free flame retardancy. However, systematic studies working out the structure property relationships are, as yet, still rare. Indeed, the deeper understanding of the actual mechanisms is rather in its infancy, as are the fundamentals for a directed development. Recently, a joint paper by American research institutes targeting aircraft applications [4] was published, comparing reactive phosphine oxides, phosphonates, and phosphates as flame retardants in epoxy systems. Part of the study presented here corresponds directly to this independently-performed study. However, the two studies are actually characterised by different approaches and represent two complementary points of view for the future discussion. The study presented here is based on a distinct systematic comparison of materials and is focussed on the mechanisms controlling pyrolysis and flame retardancy in both the condensed and the gas phases.

A comparable systematic variation of hardeners from phosphine oxide, phosphinate, phosphonate to phosphate-based ones was used to achieve reactive, halogen-free, flame-retarded epoxy resins with a consistent phosphorus content as low as around 2.6 wt.%. Systems containing phosphorus can work in the condensed phase or in the gas phase, depending on the flame retardants used and the different interactions within the multicomponent systems [5–11]. Hence, the decomposition pathways were worked out to elucidate the flame retardancy mechanisms in both the condensed phase and the gas phase actions in fire tests with respect to flammability (reaction to a small flame) and fire behaviour (forced-flaming conditions) of carbon fibre-reinforced composites. In addition, the ease of processing for liquid composite moulding technologies and the mechanical performance of the composites are addressed. Thus, the paper aims to make a valuable contribution towards a better understanding of reactive, phosphorus-containing flame retardants in epoxy resins and hence provides a foundation for the directed design of new flame-retarded, fibre-reinforced composites.

2. Experimental

2.1. Epoxy resins

Bifunctional diglycidyl ether of bisphenol A (DGEBA, Ruetapox 0162, Bakelite, commercial grade) was used. As hardeners the commercial phosphorus-free 4,4′-diaminodiphenylsulphone (DDS) and four phosphorus-containing hardeners based on diaminodiphenyl were used. DDS was provided by Merck (4,4′-DDS, Merck, synthesis grade). The phosphine oxide-based hardener (Ar_3PO) was synthesised according to Liu et al. [12]. The phosphinate-based (Ar_2PO_2), the phosphonate-based ($ArPO_3$) and the phosphate-based (PO_4) hardeners were synthesised as described in detail by Perez et al. [13]. The chemical structure of the diglycidyl ether and the hardeners used is summarised in Fig. 1.

The DGEBA was placed in a glass flask and heated to 353–363 K in an oil bath. The desired amount of hardener (molar ratio of DGEBA:hardener = 5:2 – giving an overall P-content of approximately 2.6 wt.% in the final resin and hardener mixture) was then added slowly to the resin and mixed using a mechanical stirrer for 30 min at 600–1000 rpm, keeping the temperature constant, until the mixture was homogeneous. The final mixture was poured into a preheated aluminum mould coated with a thin layer of Frekote-700 NC (for easy release of the cured specimens), degassed in a vacuum at 353 K for 30 min, and subsequently cured. The curing cycle involved a temperature increase to 453 K at a heating rate of 2 K min^{-1}, followed by an isotherm for 2 h and a slow cooling to room temperature. The resulting neat epoxy resins are referred to as EP-DDS, EP-Ar_3PO, EP-Ar_2PO_2, EP-$ArPO_3$, and EP-PO_4. The chemical compositions and molecular weight (MW) are summarised in Table 1.

2.2. Carbon fibre-reinforced epoxy composites

Composite plates of $40 \times 40 \times 2.8\ mm^3$ containing 60 vol.% of carbon fibres were manufactured using the

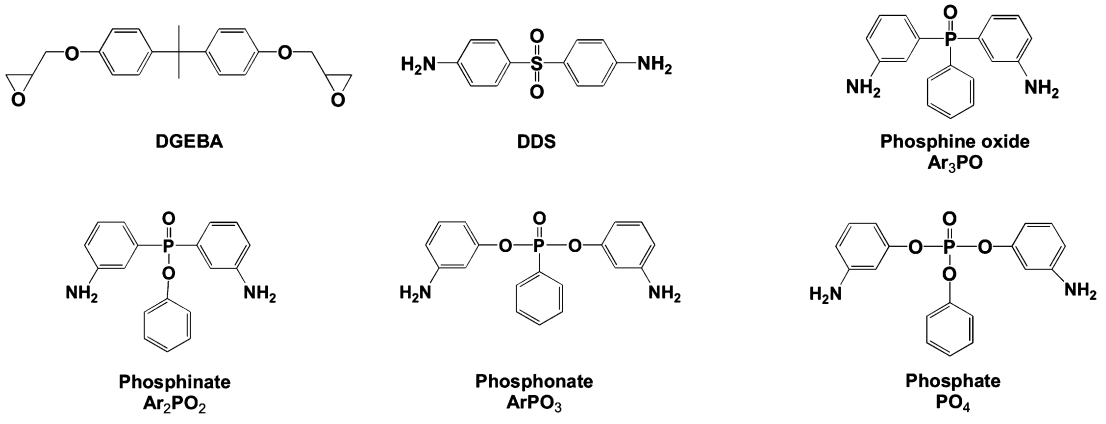

Fig. 1. Chemical structures of DGEBA and all hardeners used.

Table 1
Compositions of all neat epoxy materials

	EP-DDS	EP-Ar_3PO	EP-Ar_2PO_2	EP-$ArPO_3$	EP-PO_4
Hardener MW	248	308	324	340	356
DGEBA MW	340	340	340	340	340
EP material MW	2196	2316	2348	2380	2412
Relative composition/wt.%					
S	2.9				
C	70.5	73.1	72.1	71.1	70.1
O	17.5	15.2	16.4	17.5	18.6
H	6.6	6.6	6.6	6.5	6.4
N	2.6	2.4	2.4	2.4	2.3
P	0.0	2.7	2.6	2.6	2.6

vacuum-assisted resin transfer moulding (VARTM), or the hand lay-up technique in the case of EP-Ar_3PO. The bifunctional epoxy resin and the hardener were mixed and degassed as described above. The fibre reinforcement consisting of eight plies of woven fabric (Atlas 1/4, 5 harness satin, ECC GmbH & Co., fibre aerial weight = 370 g/m^2) was placed in the preheated RTM mould at 353–373 K. A Kapton® film of 13 μm thickness was introduced between the fourth and fifth carbon fabric as a sharp crack starter in the mid-plane of the composite area designated for further mechanical tests. The resin mixtures were preheated to the same temperature and driven into the closed RTM mould by vacuum, followed by curing at 453 K for 2 h and a slow cooling to room temperature. For easy release of the cured composite plates, the mould surface was coated with a thin layer of Frekote-700 NC. The resulting composites are referred to as EPC-DDS, EPC-Ar_3PO, EPC-Ar_2PO_2, EPC-$ArPO_3$, and EPC-PO_4.

2.3. Thermal analysis

Thermogravimetric (TG) experiments were performed using TGA/SDTA 851 (Mettler/Toledo, Gießen, Germany) applying nitrogen or synthetic air of 30 ml min^{-1}. The samples (about 10 mg) were heated in alumina pans from room temperature up to about 1200 K at heating rates of 1, 2, 5, 10 and 20 K min^{-1}. The kinetics was investigated based on the isoconversion method [14]. The TG was coupled with a FTIR Spectrometer Nexus 470 (Nicolet Instruments, Offenbach, Germany). The coupling element was a transfer tube with an inner diameter of 1 mm (heated to 523 K) connecting the TG and the infrared cell (heated to 533 K). The infrared spectrometer, equipped with a DTGS KBr detector, was operated at an optical resolution of 4 cm^{-1}. Single spectra were chosen to identify the gases evolved. The identification was based on characteristic peaks indicating chemical compounds and on comparison with reference spectra taken from a database. Product release rates were evaluated using the height of product-specific peaks as a function of time.

Solid residues collected during thermogravimetry were investigated by means of FTIR spectroscopy (FTIR Spectrometer Nexus 670/870 by Nicolet Instruments) using the Smart Golden Gate Single Reflection Diamond ATR accessory.

For performing an elemental analysis of the pyrolysis residues, an XPS analysis was carried out on a Sage 100 (SPECS, Berlin, Germany) using Mg Kα radiation and an X-ray power of 12.5 kV. A sample surface of 2 mm × 5 mm was irradiated. Single elements of the residue were identified by recording survey spectra, followed by high-resolution spectra to determine the quantity of sample using the elemental sensitivity factor method. The spectra were referenced to the binding energy of the graphitic carbon signal at 284.5 eV.

2.4. Fire testing

The flammability of the materials was determined using the limited oxygen index (LOI) according to ISO 4589 (specimen size: 6 × 3 × 100 mm^3) and the UL 94 classification (specimen size: 13 × 3 × 125 mm^3).

The fire behaviour of flaming conditions was characterised using a cone calorimeter (Fire Testing Technology, East Grinstead, UK) according to ISO 5660. This method enabled investigation with respect to heat release rate (HRR), total heat release (THR), mass loss rate (MLR), time to ignition (t_{ig}), rate of smoke release and carbon monoxide release rate. The integration of the release rates up to the end of test yields characteristics such as total heat evolved (THE, THE = THR at the end of test), total smoke production (TSR), total carbon monoxide production (TCOR), and total mass loss (TML). The flame out was defined as the end of test. Different external heat fluxes (35, 50, and 70 kW m^{-2}) were applied. All measurements were repeated. All samples (sample size: 100 mm × 100 mm × 2.8 mm) were measured in a horizontal position using a retainer frame to reduce unrepresentative edge-burning. The decreased sample area was taken into account for the calculations. The used samples are rather thin, since the investigation targets on the fire behaviour in realistic end use conditions. The samples' thickness is not suitable to determine steady state burning behaviour, but thick enough to obtain reasonable and reproducible results.

2.5. Mechanical properties of the composites

The effect of various phosphorus-containing hardeners on the interlaminar fracture toughness of the composites in mode I (tension) and mode II (shear) was evaluated using crack propagation experiments. Double cantilever beam (DCB) specimens were prepared in order to investigate the interlaminar fracture properties in mode I according to ESIS 990603, while end notched flexure samples (ENF) were used to analyse the interlaminar fracture properties in mode II according to the procedure reported in Refs. [15,16]. Five specimens for each composition were tested using a universal testing machine model Zwick Z 2.5. Short beam shear (SBS) specimens were used to determine the apparent interlaminar shear strength according to the ASTM D 2344; a minimum of four specimens was used. Flexural properties of the composites were evaluated according to ASTM D 79099. All tests were carried out at room temperature and 50% relative humidity.

3. Results and discussion

3.1. Pyrolysis: mass loss

The mass loss during decomposition of all neat epoxies is presented in Fig. 2 and the main results are further summarised in Table 2. EP-DDS released about 79% of weight in a single step with the maximum of weight loss at 678 K during experiments using a heating rate of 10 K min^{-1}. The size of this first decomposition step varies with the applied heating rate: in experiments with a lower heating rate of 1 or 2 K min^{-1}, the size of the step was only 70 wt.%. This deviation in main mass loss of about 7–9 wt.% as a function of the heating rate was observed for all DGEBA-based materials investigated and was also observed in the literature [17–19]. It is concluded that this particular behaviour is based on different competing decomposition reactions in epoxy decomposition. For a quantitative consideration and the subsequent derivation of decomposition models, the decomposition at high heating rates was used. Under these decomposition conditions, the strongly kinetics-controlled reactions, such as elimination or rearrangement reactions are less important.

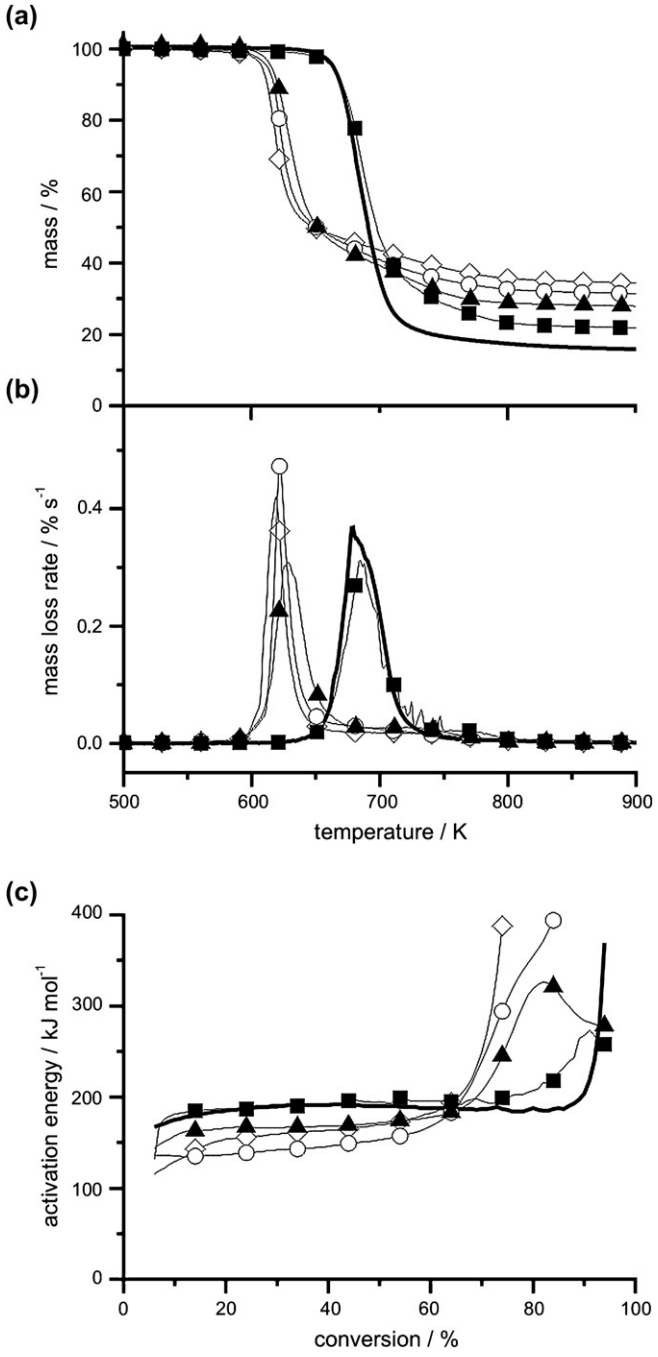

Fig. 2. TG, DTG and kinetics for all epoxy materials, 10 K min^{-1} (thick solid line = EP-DDS, filled squares = EP-Ar_3PO, filled triangles = EP-Ar_2PO_2, open circles = EP-$ArPO_3$, open rhombi = EP-PO_4).

Following the main mass loss a further mass decrease was observed until the end of the measurement, leaving a residue of 14 wt.%. The decomposition kinetics was characterised primarily by a constant activation energy of about 185–190 kJ mol^{-1}; however, during the first 20% of conversion the value was slightly lower (Fig. 2c).

Most of the EP-Ar_3PO material decomposed at a similar temperature (687 K) as the EP-DDS; however, only 65 wt.% was lost during the main decomposition step. The result, that no significant change of the decomposition temperature occurred when phosphine oxide was used, is in accordance with the literature [20–22]. A subsequent decomposition was observed up to 800 K with 12 wt.% of mass loss. The high-temperature decomposition at above 800 K corresponds to the equivalent decomposition of EP-DDS; however, the residue at 1175 K increased from around 14 wt.% up to around 19 wt.%. The activation energy showed a similar value and behaviour as for EP-DDS for a conversion of up to 80%. Beyond 80% of conversion the activation energy increased to a value above 200 kJ mol^{-1}, which is a characteristic limit for polymer/char decomposition processes.

The decomposition behaviour changed significantly for the materials containing phosphinate (EP-Ar_2PO_2), phosphonate (EP-$ArPO_3$) and phosphate (EP-PO_4). Decomposition started at lower temperatures with maxima of mass loss rate at around 620 K, and the main mass loss step decreased to values of about 51–55 wt.%. Such a decrease in decomposition temperature is characteristic for epoxy materials containing phosphonate and phosphate [23–27]. The activation energy of the decomposition step differed slightly for these materials between 140 and 160 kJ mol^{-1}; however, the deviation is on the order of magnitude of the experimental error. Compared to the EP-DDS and EP-Ar_3PO, the activation energies were lower for the main decomposition step and higher for the subsequent step between 650 and 800 K. This behaviour also has been described in the literature [26]. For all three materials a decomposition process of about 14–17 wt.% followed the main decomposition step. During these processes the activation energy showed significantly increased values. For all three materials, EP-Ar_2PO_2, EP-$ArPO_3$ and EP-PO_4, the high-temperature decomposition process between 800 and 1175 K is the same as for EP-DDS, but the residue amounts at 1175 K differed significantly. The residues increased in an ascending order from 24 to 30 wt.% with increasing oxidation of the phosphorus.

Table 2
Thermal decomposition of all EP materials at heating rate 10 K min^{-1}

	EP-DDS	EP-Ar_3PO	EP-Ar_2PO_2	EP-$ArPO_3$	EP-PO_4
Main mass loss					
ΔT/K	650–730	637–720	604–675	600–660	597–650
Δwt./%	78.8 ± 1	64.7 ± 1	54.7 ± 1	51.7 ± 1	51.1 ± 1
T_{max}/K	678 ± 2	687 ± 2	628 ± 2	621 ± 2	618 ± 2
Subsequent mass loss					
ΔT/K	730–800	720–800	675–800	660–800	650–800
Δwt./%	3.6 ± 1	12.0 ± 1	16.3 ± 1	16.7 ± 1	14.2 ± 1
High-temperature decomposition					
ΔT/K	800–1175	800–1175	800–1175	800–1175	800–1175
Δwt./%	3.2 ± 1	4.1 ± 1	5.0 ± 1	5.3 ± 1	5.9 ± 1
Residue at 1175 K					
Wt./%	14.4 ± 1	19.2 ± 1	24.0 ± 1	27.3 ± 1	29.8 ± 1

ΔT = temperature area of decomposition process, T_{max} = temperature of maximum weight change, error based on maximum deviation from average value.

3.2. Pyrolysis: evolved gas analysis

Some of the gaseous decomposition products of the EP materials were proved unambiguously by characteristic strong FTIR signals (Fig. 3), such as methane (3015 cm^{-1}), water (3854 cm^{-1}) and benzene (673 cm^{-1}). The main share of the bands of the decomposition products is attributed to the functional groups with characteristic, unambiguous band positions: compounds containing carbonyl (~1745 cm^{-1}) and phenol (745 cm^{-1}), and methyl-substituted compounds (2968 cm^{-1}).

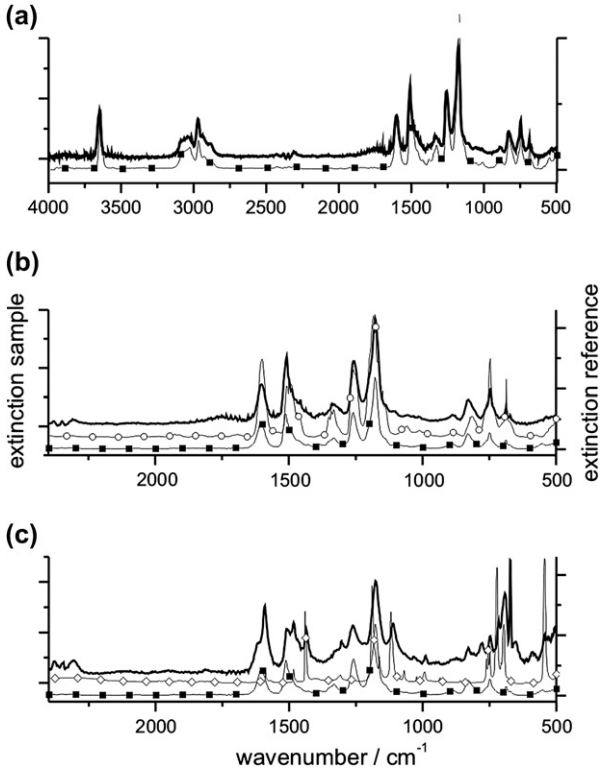

Fig. 3. Characteristic evolved gas analysis spectra of $OPAr_3$ at 40 (a, b) and 48 min (c) with reference spectra from a database (thick solid line = sample spectra, filled squares = bisphenol A, open circles = phenol, open rhombi = triphenylphosphine oxide). Remaining bands around 1745 cm^{-1} (a, b) are attributed to carbonyl derivatives and at 673 cm^{-1} (c) to benzene.

It is assumed, and also described in the literature [2,22,25,28,29], that these signals originate from a number of specific decomposition products: for example the phenol signal at 745 cm^{-1} originates from such compounds as methyl phenol, ethyl phenol, and isopropyl phenol.

Under thermal decomposition conditions for EP-DDS sulfur dioxide (1375 cm^{-1}), water, carbon monoxide (2175 cm^{-1}) and methane were verified as gaseous decomposition products as well as fragments containing phenol (for example, phenol and bisphenol A) and components containing carbonyl (for example, acetone). All decomposition products were released with similar product release rates around 40 min, which correspond to the main decomposition process of EP-DDS.

If the phosphorus-containing hardener replaces the DDS hardener, sulfur dioxide disappears as a decomposition product. Apart from the SO_2 release the evolved gas analysis spectra match the spectra of EP-DDS, hence the main decomposition products were not changed in principle. However, slight differences existed for the different phosphorus components, especially in the product release rates.

For the phosphine oxide-based material (EP-Ar_3PO) an additional triphenylphosphine oxide signal was observed (1484, 1436, 1111 cm^{-1}, see Fig. 3c) during the complete decomposition, and benzene release during the subsequent decomposition process at above 650 K. The occurrence of both decomposition products proved that EP-Ar_3PO releases part of the phosphorus in the gas phase while part of the phosphorus remains in the residue.

The product release rates of the characteristic peaks of the epoxy matrix, such as the phenol, bisphenol A, carbonyl, and water signals, showed no deviation from those for EP-DDS. The decomposition of ether bonds is not influenced.

Compared to EP-DDS, the pyrolysis of epoxy materials containing phosphinate (EP-Ar_2PO_2) and phosphate (EP-PO_4) did not produce any additional decomposition products, whereas additional benzene was observed for the material containing phosphonate (EP-$ArPO_3$). For all the phosphorus components containing phenoxy the product release rate of water increased, whereas the carbonyl and methane release rates decreased during the main decomposition. An increase in

methane and phenol release was observed in the subsequent decomposition step. The materials containing phenoxy side groups, EP-Ar_2PO_2 and EP-PO_4, also showed an increased phenol release during the main decomposition process, whereas EP-$ArPO_3$, which possesses a phenyl side group, released benzene, especially during the subsequent decomposition process. Thus, the phenol release as well as the benzene release corresponds to their characteristic decomposition temperatures observed in thermal analysis, which is lower for P–O–C (aromatic) than for P–C (aromatic).

The decomposition products of the materials containing a phenoxy group, EP-Ar_2PO_2, EP-$ArPO_3$ and EP-PO_4, indicate that the change in the thermal decomposition behaviour as observed for these materials by thermogravimetry is accompanied by an enhanced water elimination process instead of carbonyl release. Furthermore, some of the aromatics and methane remain in the residue during the main decomposition process and are released in subsequent decomposition processes at higher temperatures. The results of the pyrolysis products release correspond well to thermal analysis and are explained by the proposed decomposition models discussed below.

3.3. Pyrolysis: residue

Residues obtained in TG by heating the sample to a desired temperature or weight loss were subjected to the FTIR analysis. The FTIR spectra of the initial EP-PO_4 and of its solid pyrolysis products are shown as an example in Fig. 4, reflecting an increasing degree of conversion. Analogous experiments were performed for all the materials. Based on the characteristic IR frequencies, key groups were identified. Their decomposition or formation was monitored by means of the intensity of the absorption bands with the progression of pyrolysis.

By heating to 7% weight loss, the EP-DDS sample showed a weak absorption band at 1645 cm^{-1} due to the olefinic C=C bond, indicating dehydration of the 2-hydroxytrimethylene structure during the initial stages of degradation to yield the allylic one. The band disappeared upon further heating to 15% weight loss, obviously due to the decomposition of the allylic structure and subsequent volatilisation. Simultaneously, a decrease in the intensity of the OH– (3400 and 1080 cm^{-1}, shoulder) and $-C_6H_4-O-CH_2-$ (1224 and 1028 cm^{-1}) related absorption bands was observed, as well as that of the aromatic 1507 cm^{-1} band, which continued steadily to 79% weight loss, indicative of volatilisation of the 2-hydroxytrimethylene and bisphenol A units. Concurrently with this event, the intensity of the absorption bands due to secondary amines (3370 cm^{-1}), and due to $-SO_2-$ (1289 and 1141 cm^{-1}), increased, showed their maximum intensity at 55% weight loss and then declined by heating to 79 and 83% weight losses, associated with an accumulation and decomposition of the hardener structure. The 1102 cm^{-1} band followed the same trend. In contrast to the 1507 cm^{-1} band, the 1591 cm^{-1} aromatic band persisted heating to 83% weight loss and broadened, indicating polyaromatisation of the solid residue. The other important absorption bands observed in the residue at 83% weight loss were aliphatic CH-bonds (2960–2863, 1440 cm^{-1}, weak-to-medium intensity), carbonyls (1740–1700 cm^{-1}, weak), aromatic ethers (1255 cm^{-1}, weak), and phenols (3600–3200 cm^{-1}, weak and broad). The presence of phenols is also suggested by the characteristic triplet at 871, 807 and 744 cm^{-1}.

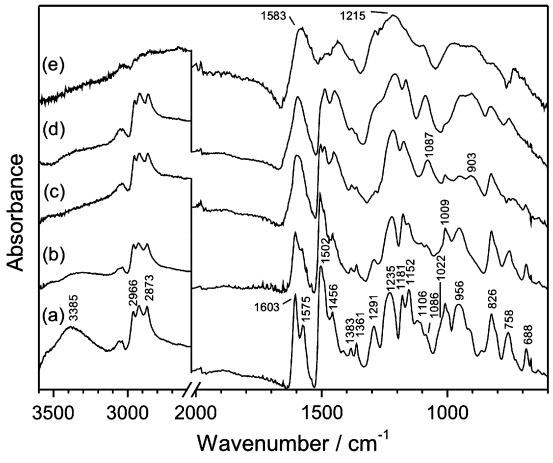

Fig. 4. FTIR spectra of initial EP-PO_4 (a) and of its solid products of thermal decomposition obtained under nitrogen in TG by heating to 10% weight loss (b); 35% weight loss (c); 53% weight loss (d) and to 768 K.

Through heating to 74% weight loss, the EP-Ar_3PO sample showed a steady decrease in the absorption bands of OH (3304 and 1085 cm^{-1}), the aromatic ring (1508 cm^{-1}), $-C_6H_4-O-CH_2-$ (1225 and 1028 cm^{-1}), $C(CH_3)_2$ (1384, 1362, 1181 cm^{-1}), H–C (aromatic) (827 cm^{-1}), indicating decomposition and volatilisation of the 2-hydroxytrimethylene and bisphenol A structures. Formation of the olefinic bond (characteristic absorption band at 1645 cm^{-1}) and of the secondary amine (characteristic absorption band at 3370 cm^{-1}) was not observed. In addition, there was an increase in the intensity of the absorption bands at 1439 cm^{-1} (P–C_6H_4), 1178 cm^{-1} (P=O) and 1111 cm^{-1} (partially due to aliphatic polyether structures, and probably due in part to P–Ar_3, as the band is observed in the IR spectrum of initial Ar_3PO), indicating accumulation of the hardener. However, these absorption bands decreased upon further heating to 838 K, indicative of volatilisation of phosphorus-containing products and decomposition of the polyether units. The char obtained at this temperature was of a polyaromatic character, as revealed by the broadening of the 1583 cm^{-1} absorption band.

All of the other three samples, EP-Ar_2PO_2, EP-$ArPO_3$ and EP-PO_4, also showed decomposition and volatilisation of the 2-hydroxytrimethylene and bisphenol A units through heating to the end of the main stage of weight loss, with the subsequent polyaromatisation of the solid decomposition products. For the EP-PO_4 sample (Fig. 4), for example, these changes can be followed by a decrease in the intensities at 3385 cm^{-1} (OH), 1086 cm^{-1} (C–OH), 1502 cm^{-1} (aromatic ring), 1381, 1361 and 1181 cm^{-1} ($C(CH_3)_2$), 1235 and 1022 cm^{-1} ($-C_6H_4-O-CH_2-$), and a broadening of the 1603 cm^{-1} band. No absorption band due to secondary amines is observed.

However, the three samples exhibit rapid disappearance of the broad absorption band at 3600–3200 cm^{-1}, associated

with vibration of the hydrogen-bonded hydroxyl group, indicating a completely different decomposition mechanism of the substances.

Concurrently with the decomposition of the OH group, the rapid disappearance of the absorption bands due to P–O–C (aromatic) is also observed, as shown for EP-PO_4 (1152 and 956 cm^{-1}, Fig. 4 spectra b and c). Simultaneously, a new absorption band appears in the case of EP-Ar_2PO_2 at 1036 cm^{-1} (at 10 and 27% weight loss), and in the case of EP-$ArPO_3$ at 1045 cm^{-1} (at 15 and 30% weight loss), ascribable to the P–O–C (aliphatic) stretching vibration. The new absorption band disappears upon further heating, with the production of absorption bands at about 900 cm^{-1} (P–O–P) and 1090 cm^{-1}. The 1090 cm^{-1} band is not assigned; however, it often appears in the IR spectra of structures containing –P–O–P–O, especially in those of ionised compounds [30]. For example, the two bands around 900 and 1090 cm^{-1} are present in the IR spectra of melamine polyphosphate or ammonium polyphosphate. Through further heating to 700 K the 900 and 1090 cm^{-1} bands initially increase in intensity and then decline.

In the case of EP-PO_4 the production of an absorption band due to the P–O–C (aliphatic) ester bond is not detected; however, those due to the structures containing –P–O–P–O lie at 1087 and 903 cm^{-1} (Fig. 4, spectra c–e). The formation of pyrophosphates may be responsible for the broadening of the absorption band between 1300 and 1250 cm^{-1} due to the stretching vibration of the P=O group.

Finally, the study revealed modification of the absorption band of the phosphoryl group P=O in EP-Ar_2PO_2, EP-$ArPO_3$ and EP-PO_4, best highlighted for EP-PO_4 in Fig. 4. Through heating there is a decrease in the intensity of the absorption band at 1291 cm^{-1} due to P=O, caused by decomposition of the phosphate hardener. A new absorption band at 1215 cm^{-1} appears, ascribable to the P=O stretching vibration in amidophosphates (O=P–N) [30] or the P=N stretching vibration in their condensation products such as $(PON)_x$. The amidophosphates can be formed either through reaction of a P–O–C bond with a secondary amino group or through reaction of amino group with the structures containing –P–O–P–O.

In conclusion, the formation of a P–O–C (aliphatic) bond is indicative of the reaction of a P–O–C (aromatic) bond with a secondary OH group. This reaction may be catalysed by a secondary amino group due to the formation of organophosphorus products containing P–N (amidophosphates, for example). Their formation dominates at the end of the main stage of weight loss, together with the polyaromatisation processes of the solid residue. The secondary amines needed for the aminolysis reaction of the hardeners can be present in the initial epoxy resin or result from its decomposition.

3.4. Pyrolysis: decomposition models

On the basis of the results for mass loss, volatile products, residue and decomposition kinetics, models are postulated and summarised for the main decomposition pathway for EP-DDS and EP-Ar_3PO in Fig. 5 and for the phenoxy-containing epoxy resins in Fig. 6, using the example of EP-PO_4.

Fig. 5 describes the main decomposition pathway of EP-DDS and EP-Ar_3PO. The initial compound illustrated is a cut-out of the EP structure; however, the discussion regarding the mass loss (Table 3) considers the complete structure of the absolute stoichiometric rate of DGEBA/hardener of 5:2. The epoxy network breaks first at nitrogen bonds, because the binding force of nitrogen–aliphatic carbon bonds is lower than the binding force of carbon–carbon and carbon–oxygen bonds [2,22]. The sulfur dioxide vaporises, as do acetone and most of the aromatic compounds containing oxygen and nitrogen. The sum of the molecular weights of these proposed decomposition products during the main decomposition step amounts to a theoretical mass loss of 81 wt.%, which corresponds to the experimental value of 79 wt.% (Table 3). After the main decomposition step, hydrogen-poor carbon components remain, which degrade further until the end of the measurement, vaporising methane and carbon monoxide. A graphite-like residue of 15 wt.% remained at 1175 K, which corresponds to the experimental value of 14 wt.%.

This decomposition models (Fig. 5) consider the vaporisation of acetone and disregards the elimination of water from secondary hydroxyl groups; although this alternative process was also proved unambiguously through residue and evolved gas analysis. This assumption regarding the sole vaporisation of acetone as a placeholder for both reactions is allowed as these two different pathways do not change the main process of decomposition of aromatics, which are the main contributors of mass; therefore the switch between the pathways changes the charring process only slightly. A similar simplification was also done for the release of phenol and bisphenol A. Here, the major decomposition to bisphenol A and the minor decomposition to phenol were considered, although no quantitative results exist for the relative rates of both. The decomposition model also confines itself to describe the main principle decomposition pathway. However, there are relevant minor decomposition pathways for the epoxy network structure. As an example in all residues a significant trace of nitrogen was found by XPS indicating that the release of nitrogen is not complete.

When the phosphine oxide-based hardener replaces the DDS hardener (EP-Ar_3PO) the main decomposition pathway changes slightly (Fig. 5). SO_2 disappears as a decomposition product. The bisphenol A, phenol and acetone rates are not affected, and neither are methane and CO release during the subsequent degradation process beyond 725 K. Instead of the vaporisation of methylaniline in EP-DDS, for EP-Ar_3PO the vaporisation of methylamine and triphenylphosphine oxide is proposed. The quantitative analysis proved (Table 3) that the decomposition of the phosphorous component contributed to both decomposition steps. The experimental mass loss steps of 65 wt.% and of 16 wt.% correlated well with the sum of the calculated mass loss steps of 53 wt.% and of 33 wt.%. The residue of 19 wt.% determined in the experiment was larger than the calculated value of 14 wt.%. The detailed analysis of decomposition also demonstrated benzene as a decomposition product and phosphoryl components in the residue. Consequently, an alternative minor decomposition pathway

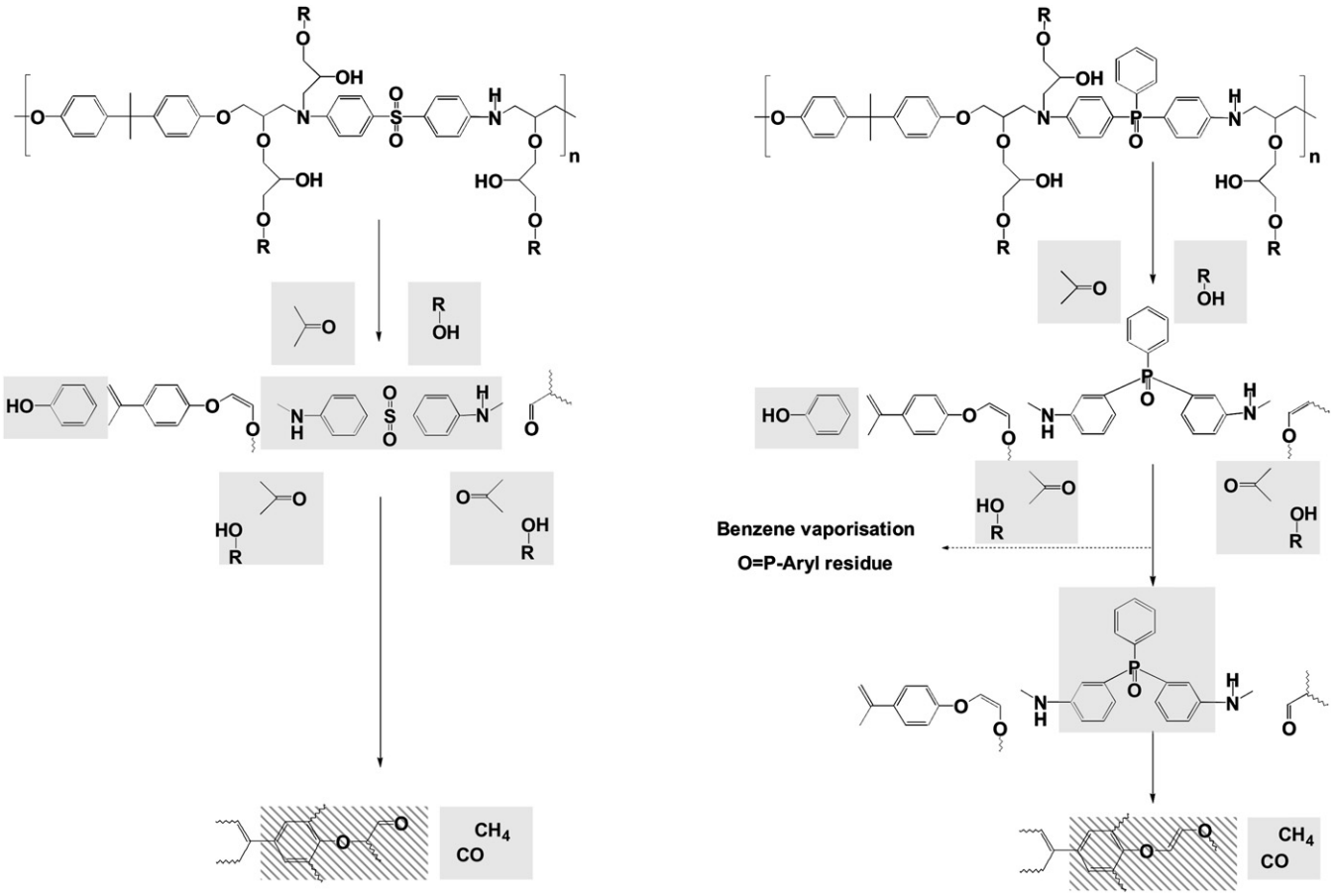

Fig. 5. Decomposition model of EP-DDS and EP-Ar_3PO (n = molecular structure of simplified monomer unit, R = connection to bisphenol A units, zig-zag line = cross-linking/char formation, grey background = proved gaseous decomposition products, dashed background = proved residue structures).

is presumed in which triphenylphosphine oxide units decompose, decreasing the decomposition steps and increasing the residue amount. Thus, the main decomposition pathway results in the release of phosphorus-containing volatiles, whereas traces of the phosphorus remain in the condensed phase due to a side decomposition pathway.

Compared to EP-DDS and EP-Ar_3PO, the use of the materials containing phosphinate (EP-Ar_2PO_2), phosphonate (EP-$ArPO_3$) and phosphate (EP-PO_4) lowered the decomposition temperature and activation energy, and decreased the main decomposition step significantly. The kind of decomposition products was not changed significantly; hence the phosphorus compounds facilitate the decomposition process of the epoxy matrix and suppress part of the decomposition process. For all three materials this is due to corresponding phosphorus-containing acids produced in the reaction of the secondary hydroxyl groups with the phenoxy groups of the hardener also resulting in the formation of phenol species and double bonds. The phosphorus-containing acids produce water to condense to polyphosphates. Hence, EP-Ar_2PO_2, EP-$ArPO_3$ and EP-PO_4 induced the water elimination instead of the acetone vaporisation of epoxy, accumulating carbon char in the solid residue. As this reaction is enhanced through the increasing oxidation of the phosphorus, the char residue increases in the order phosphinate < phosphonate < phosphate. Further, the formation of amidophosphates (-phosphonates) becomes more important as decomposition progresses, thus retaining nitrogen in the residue, which was also proved. The formation of polyphosphate is not considered in the quantitative analysis of the mass loss; however, the formation of P_2O_5 or $P_2O_3N_2$ instead of P_2O_8 or $P_2O_6N_2$ does not change the result significantly.

For the main decomposition step of EP-Ar_2PO_2, EP-$ArPO_3$ and EP-PO_4, theoretical mass loss values of 48, 61 and 51 wt.%, respectively, are calculated due to the volatilisation of bisphenol A, phenol, acetone and water (Table 3). The step sizes strongly depend on the non-bridged substituent at the phosphorus atom and on the relative rate of acetone and water release according to the oxidation state of phosphorus. The release of aniline species is delayed to the subsequent decomposition steps, which amounted to 17, 26 and 19 wt.% for the materials. Through TG, mass losses of 55, 52 and 51 wt.% in the main decomposition step and those of about 21 wt.% in subsequent decomposition steps were proved for all three materials. An excellent correlation was found for EP-PO_4, the decomposition model of which is illustrated in Fig. 6. Each P–O–C group initiates the vaporisation of water instead of acetone, resulting in the formation of a P–OH group. These acid groups are able to form ammonium salts and, consequently, enhances the retaining of nitrogen in the condensed phase. In the subsequent decomposition step, the remaining acid groups

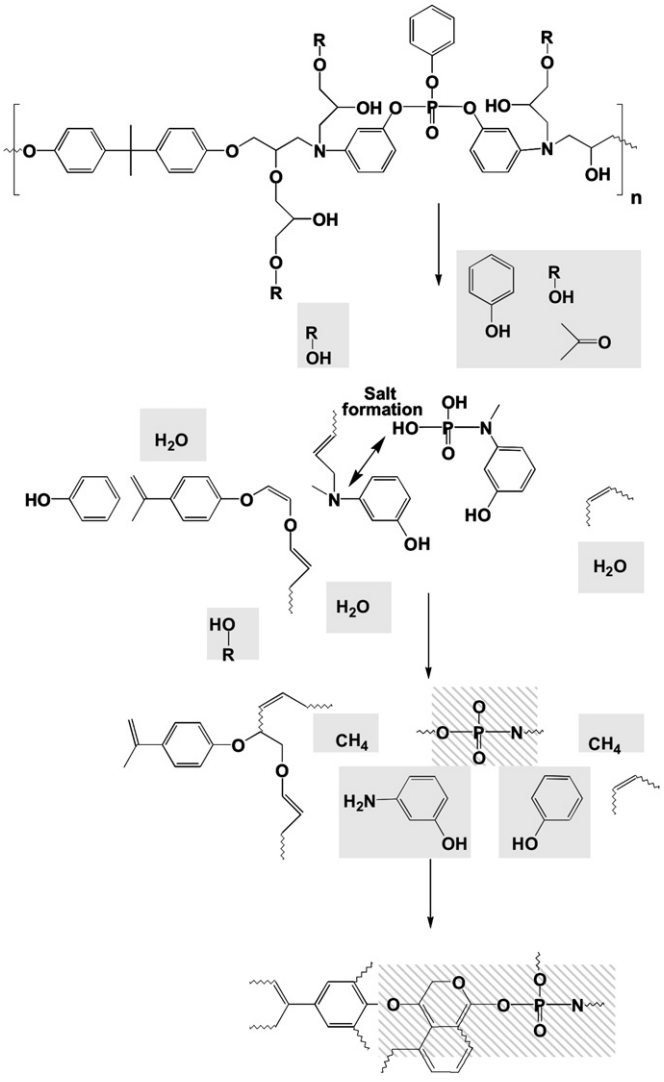

Fig. 6. Decomposition model of EP-PO_4 (n = molecular structure of simplified monomer unit, R = connection to bisphenol A units, zig-zag line = cross-linking/char formation, grey background = proved gaseous decomposition products, dashed background = proved residue structures).

form polyphosphates. Nitrogen–aliphatic carbon bonds are cut, resulting in the additional release of aromatics and methane. For EP-Ar_2PO_2 and EP-$ArPO_3$ consistent decomposition models were developed; the deviations are probably based on partial vaporisation of the species containing phosphorus.

For EP-$ArPO_3$ additional elemental analysis of homogenised residues at 773 K was performed using XPS, which proved a composition of $C_{40}O_4N_2P_2$. The residue at 773 K amounts to 35 wt.%, which is about 8 wt.% higher than the residue at 1175 K. Taking into account the further release of small hydrocarbons and aromatics between 773 and 1175 K and the formation of polyphosphates instead of phosphates, the proposed composition of $C_{32}O_8N_2P_2$ was approximated.

3.5. Fire behaviour: ignition and flammability

Pyrolysis indicated different phosphorus-release and charring characteristics for the different EPs, and thus specific flame retardancy mechanisms were expected to be active in the gas phase and condensed phase for each carbon fibre-reinforced EP composite. The resulting performance of the composites was investigated with respect to ignitability and flammability (reaction to a small flame) and fire behaviour (forced-flaming condition).

The time to ignition (t_{ig}) obtained in the cone calorimeter shows clear differences in the ignition behaviour of the various samples (Table 4). It is in the following order: EPC-Ar_3PO - < EPC-Ar_2PO_2 = EPC-$ArPO_3$ = EPC-PO_4 ≤ EPC-DDS. This result corresponds well to the decomposition temperatures and product release rates during thermal decomposition of EP-Ar_2PO_2, EP-$ArPO_3$, EP-PO_4, and EP-DDS, but not in the case of EP-Ar_3PO (Table 2). The shorter ignition time for EPC-Ar_3PO may be due to a minor homogeneity or curing obtained by the manual composite lay-up technique which was necessary for processing this particular material.

The flammability behaviour of the various composite materials in terms of LOI and UL 94 results is summarised in Table 4. The LOI increased by up to a difference of 8%, which corresponds to the order of magnitude improvement reported in the literature for epoxy materials containing phosphate (6–8%) and phosphonate (5–7%) [24–26,31–33]. EPC-PO_4 has the lowest LOI of 29% and EPC-Ar_3PO the highest of 39%. The significant influence of phosphine oxide on LOI again is in agreement with the literature [34,35], where increases of 10% have been reported for a phosphine oxide-based epoxy material. The LOI of EPC-PO_4 was even lower than EPC-DDS, indicating a significant contribution of the –SO_2– group [25,35] towards obtaining a reduced flammability even better than the one observed for the phosphorus-containing materials. The LOI performance of the different materials is ordered as: EPC-Ar_3PO > EPC-$ArPO_3$ ≥ EPC-Ar_2PO_2 > EPC-DDS ≥ EPC-PO_4.

In agreement with these LOI results, only EPC-Ar_3PO passes the vertical UL 94 test with a classification of V-1, whereas all the other materials tested were classified as HB. The fact that only materials with high LOI values, as of around 40, pass the UL 94 test is characteristic for composites, where effects such as wicking or suppression of an effective barrier formation occur [35,36]. In agreement with the decomposition models, it was concluded that the flammability results are controlled in particular by the gas phase action due to the release of phosphorus-containing volatiles, whereas the difference in the charring of the materials seems to play a negligible role. Hence, EPC-PO_4 performed even worse than EPC-DDS, since all the phosphorus remains in the condensed phase. EPC-Ar_3PO showed the best performance because the majority of the phosphorus is released, whereas EPC-Ar_2PO_2 and EPC-$ArPO_3$ perform somewhere in between.

3.6. Fire behaviour: flaming conditions

The results of cone calorimeter investigations are illustrated in Figs. 7 and 8 and Table 5. Fig. 7 presents characteristic heat release rate and total heat release curves at an external heat

Table 3
Calculated and experimental decomposition steps of all neat epoxy materials

	EP-DDS	EP-Ar_3PO	EP-Ar_2PO_2	EP-$ArPO_3$	EP-PO_4
Main mass loss/wt.% (number of molecules)					
SO_2	5.8 (2)				
Bisphenol A	31.1 (3)	29.5 (3)	29.1 (3)	28.7 (3)	28.4 (3)
Phenol	8.6 (2)	8.1 (2)	16.0 (4)	7.9 (2)	15.6 (4)
Methylaniline	19.3 (4)				
Acetone	15.8 (6)	15.0 (6)	14.8 (6)	9.7 (4)	4.8 (2)
H_2O			0.8 (1)	1.5 (2)	2.2 (3)
Σwt. (calc.)	80.7	52.7	60.7	47.9	51.0
Σwt. (exp.)	78.8	64.7	54.7	51.7	51.1
Subsequent mass loss + high-temperature decomposition/wt.% (number of molecules)					
Aromatics			14.1 (4)	16.8 (4)	16.7 (4)
Benzene				6.6 (2)	
P-component[a]		29.0 (2)			
CH_4	2.9 (2)	1.4 (2)	2.7 (4)	2.7 (4)	2.7 (4)
CO	2.6 (2)	2.5 (2)			
Σwt. (calc.)	4.1	32.9	16.9	26.1	19.4
Σwt. (exp.)	6.8	16.1	21.3	22.0	20.1
Residue/wt.%					
Composition	$C_{22}O_6$	$C_{22}O_6$	$C_{26}O_8N_2P_2$	$C_{32}O_8N_2P_2$	$C_{38}O_{10}N_2P_2$
Wt. (calc.)	14.9	14.2	24.5	25.3	29.3
Wt. (exp.)	14.4	19.2	24.0	27.3	29.8

[a] Triphenylphosphine oxide + methylamine.

Table 4
Time to ignition and flammability behaviour

	EPC-DDS	EPC-Ar_3PO	EPC-Ar_2PO_2	EPC-$ArPO_3$	EPC-PO_4
t_{ig} (at 35 kW m^{-2})/s	122 ± 2	79 ± 10	105 ± 5	106 ± 3	107 ± 1
LOI/%	31 ± 1	39 ± 1	34 ± 1	36 ± 1	29 ± 1
UL 94	HB	V-1	HB	HB	HB

t_{ig} from cone calorimeter investigations.

flux of 50 kW m^{-2}, Fig. 8 and Table 5 summarise the characteristic results of all measurements.

The HRR curve of the residue-forming and charring materials EPC-DDS, EPC-Ar_3PO, EPC-Ar_2PO_2, EPC-$ArPO_3$, and EPC-PO_4 showed a shape that is normally rather typical for non-charring samples of intermediate thickness (Fig. 7). There is an initial increase in HRR up to a shoulder, followed by a dominant peak of HRR at the end of burning. Only the HRR curve for the material with the lowest char yield, EPC-Ar_3PO, showed a behaviour in which, after the initial increase, the HRR shoulder also turned into a peak of HRR followed by a decrease in HRR, which is somewhat typical for

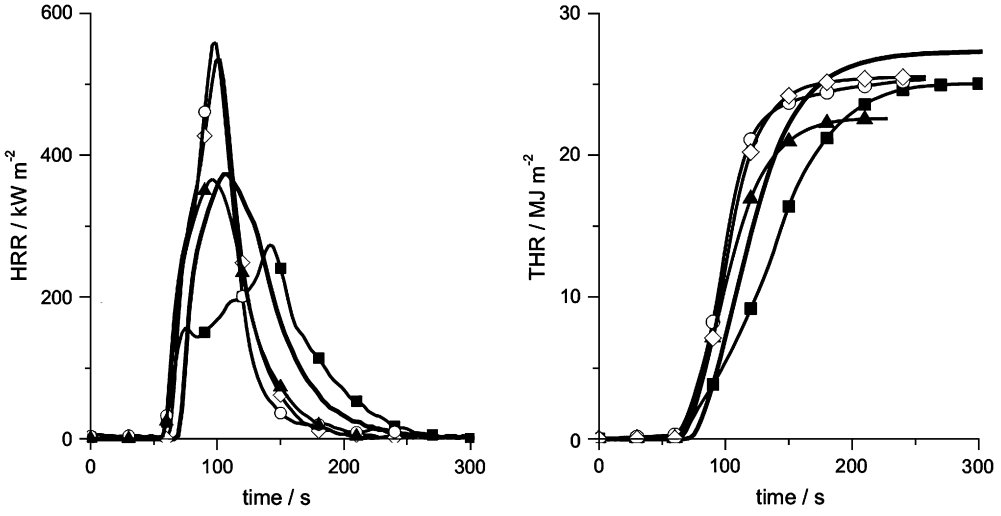

Fig. 7. Heat release rate and total heat release of cone calorimeter measurements with 50 kW m^{-2} external heat flux (thick solid line = EPC-DDS, filled squares = EPC-Ar_3PO, filled triangles = EPC-Ar_2PO_2, open circles = EPC-$ArPO_3$, open rhombi = EPC-PO_4).

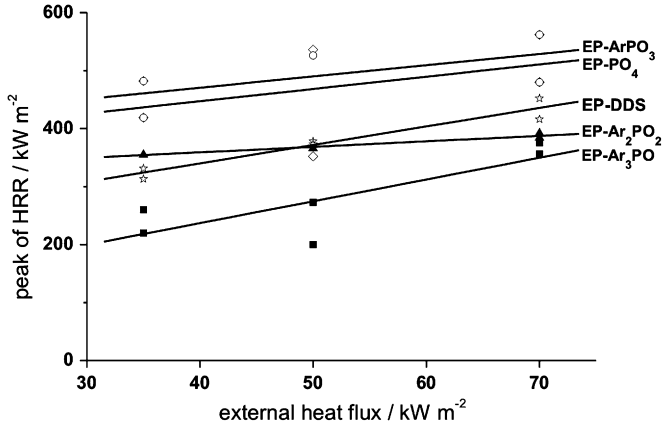

Fig. 8. Peak of heat release rate (peak of HRR), as observed by cone calorimeter measurements using different external heat fluxes, all data averaged (open stars = EP-DDS, filled squares = EP-Ar_3PO, filled triangles = EP-Ar_2PO_2, open circles = EP-$ArPO_3$, open rhombi = EP-PO_4).

char-forming materials. This starting principle change in HRR curve during burning may be also indicated by the dependence of the peak of HRR on external heat flux (Fig. 8), for which only EPC-Ar_3PO showed a reduced slope that indicated stronger barrier effects [37]. However, the dominant peak of HRR at the end of burning indicated that no efficient barrier for heat transport controlled the burning. It is concluded that this remarkable observation – that despite a high residue yield of as high as 75 wt.% no typical char-forming burning behaviour was observed – is due to the influences of the high carbon fibre content of 60 vol.% and the low specimen thickness of 2.8 mm. Most likely, both effects, the high filler content and the low thickness, together resulted in the minor impact of the charring properties of the investigated materials on the fire behaviour. And indeed, apart from the lower residue obtained for EPC-Ar_3PO, the difference in residue is hardly significant considering the data error and the fact that 80–87% of the remaining residue is given by the fibre content. In particular, the EPC-DDS material showed an amount of residue after flame out twice higher than that can be expected from the thermal analysis of the neat resins. It becomes clear that EPC-DDS is not a perfect phosphorus-free material to use for comparison in terms of a systematic variation of the chemical structure. However, EPC-DDS reflects the performance of an established system to compare with. The $-SO_2-$ group had a significant impact on the decomposition in the condensed phase and a fuel-dilution effect in the flame zone. These effects vanished for the phosphorus-containing materials due to the replacement of the $-SO_2-$ group, but not due to the use of a phosphorous group. The char yields of the materials containing phosphorus were found in an order similar to that of the residues obtained by thermal analysis: EPC-Ar_3PO < EPC-$ArPO_3$ ≤ EPC-DDS < EPC-Ar_2PO_2 = EPC-PO_4.

Compared to the EPC-DDS system, EPC-Ar_3PO showed a clear reduction in HRR and peak of HRR of around 27% (Figs. 7 and 8). At the same time no increase, but a reduction in char yield was observed (Table 5). The total heat evolved per total mass loss (THE/TML) is a measure for the effective heat of combustion of the volatiles, multiplied by the combustion efficiency during the cone calorimeter test. The THE/TML for EPC-Ar_3PO showed a reduction by about a quarter in comparison to EPC-DDS, which unambiguously indicated a flame inhibition effect as the main fire retardancy mechanism. This result corresponds with the pyrolysis behaviour indicating the vaporisation of phosphorus and the flammability behaviour indicating a dominant gas phase mechanism. No significant change in THE was observed for the investigated specimens due to the counterbalancing effects of flame inhibition, increased mass and reduced char yield.

EPC-Ar_2PO_2 showed an HRR and peak of HRR similar to those of EPC-DDS. For EPC-$ArPO_3$ and EPC-PO_4, the HRR and especially the peak of HRR were clearly increased. THE for EPC-Ar_2PO_2 showed a slight reduction, whereas no

Table 5
Averaged cone calorimeter data measurements with 35, 50 and 70 kW m^{-2} external heat fluxes (ext. HF)

Sample	Ext. HF (kW m^{-2}, ±0.2)	Mass (g, ±0.8)	Peak of HRR (kW m^{-2}, ±60)	THE (MJ m^{-2}, ±3)	Residue (%, ±3)	THE/TML (MJ m^{-2} g^{-1}, ±0.1)	TSR/TML (g^{-1}, ±6)	TCOR/TML (g g^{-1}, ±0.01)
EPC-DDS	35	42.3	322	23.3	74.8	2.2	120	0.05
	50	42.0	375	24.3	74.8	2.2	127	0.05
	70	42.0	434	25.7	72.5	2.2	98	0.05
EPC-Ar_3PO	35	45.1	240	25.0	68.1	1.7	183	0.11
	50	45.7	237	20.5	72.2	1.6	219	0.12
	70	44.7	366	26.5	66.0	1.7	218	0.11
EPC-Ar_2PO_2	35	43.6	355	21.5	76.6	2.1	143	0.08
	50	43.3	366	21.5	76.9	2.1	149	0.08
	70	43.0	388	21.3	74.9	2.0	174	0.08
EPC-$ArPO_3$	35	44.8	450	23.2	73.7	2.1	129	0.11
	50	49.1	536	24.5	73.0	2.0	170	0.12
	70	44.4	521	23.4	73.2	1.9	168	0.11
EPC-PO_4	35	44.3	529	21.6	76.9	2.0	97	0.09
	50	45.3	623	25.6	75.3	2.3	98	0.10
	70	45.2	573	25.1	75.5	2.2	92	0.09

Error based on the maximum deviation from single averaged values.

reduction was observed for EPC-$ArPO_3$ and EPC-PO_4. The peak of HRR for all the investigated materials are ordered by increasing fire risk: EPC-Ar_3PO < EPC-Ar_2PO_2 = EPC-DDS < EPC-$ArPO_3$ = EPC-PO_4. The flame inhibition for all the investigated materials is ordered as: EPC-Ar_3PO > EPC-$ArPO_3$ = EPC-Ar_2PO_2 ≥ EPC-PO_4 = EPC-DDS. This result corresponds well to the phosphorus vaporisation potential during pyrolysis investigated with the thermal analysis.

The result that phosphate worked exclusively in the condensed phase is in agreement with the literature. For epoxy materials flame-retarded with phosphates a reduction in peak of HRR and THE was reported [31,32,38], the latter on the same order of magnitude as the residue increased. The improvement was also due to the solid-state action of phosphate. Comparable studies on phosphorus-containing flame retardants of various oxidation states are rare. However, in vinyl acetate/butyl acrylate copolymers [39], the solid phase action of phosphate and the partial gas phase action of phosphonate were proved, in agreement with the result of this work. Comparison with a reported polystyrene system [40] is difficult because of experimental limitations; however, the relative reduction in THE was reported in a descending order: phosphate > phosphonate > phosphine oxide at mainly constant amounts of residue, indicating an increasing gas phase action with decreasing oxidation state of the phosphorus. Comparing the result of this study with the work of Hergenrother et al. on epoxy resins containing different kinds of phosphorous flame retardants [4] reveals some agreement but also important additional information. The increase in the condensed phase action of phosphorus with the increasing oxidation of phosphorus was found in both studies. Yet the increase of flame inhibition with decreasing oxidation was observed clearly and underlined as the more important flame retardancy effect for composites in this study only.

Apart from the heat release characteristics, the smoke and CO releases (Table 5) are important fire hazards. Furthermore, they also often indicate the fire retardancy mechanisms. Flame inhibition results in an increase in combustion products typical for incomplete combustion, in particular CO. For the investigated materials containing phosphorus, an increase in both total smoke release and total smoke release/total mass loss was observed in the following order: EPC-PO_4 < EPC-DDS < EPC-Ar_2PO_2 = EPC-$ArPO_3$ < EPC-Ar_3PO. The ranking correlates to the ranking of the flame inhibition effect. CO production showed a similar ranking, with total CO release and total CO release/mass loss increasing in the following order: EPC-DDS < EPC-Ar_2PO_2 < EPC-PO_4 ≤ EPC-$ArPO_3$ = EPC-Ar_3PO. The results also reflect the gas phase action of phosphorus, with the exception of the EPC-Ar_2PO_2 material.

3.7. Mechanical properties of the carbon fibre-reinforced composites

As such modified epoxy resins are intended for use as matrices for the manufacture of fibre-reinforced composites prepared using liquid composite moulding technologies for demanding applications in the transportation sector, a comparative assessment of their processing behaviour as well as of the resulting composite properties is required. Actually, it is almost a general drawback of flame retardants that their incorporation deteriorates the mechanical properties. Hence, the accomplishment of sufficient performance in terms of both key mechanical properties and performance under fire is the crucial challenge for the fibre-reinforced composites. The following section therefore provides a brief overview of some key mechanical properties of the investigated composites; a detailed description of the processing behaviour, the curing kinetics as well as of all relevant properties is presented elsewhere [13]. The summary presented here is set in relation to the effectiveness of the various phosphorus hardeners in terms of the flame retardancy in order to further stimulate the discussion on this particular approach towards establishing future strategies for flame-retarded high-performance composites.

Composite processing and infiltration of the fibre reinforcement using EP-PO_4, EP-DDS, EP-Ar_2PO_2 or EP-$ArPO_3$ did not pose any difficulties at the selected injection conditions (1 bar and 353–373 K). At such injection temperatures the viscosity and reactivity of the resin formulations were low enough to provide an adequate processing time to fully impregnate the fibres and fill the mould. The good quality and homogeneity of these composite plates were further verified by means of ultrasonic C-Scans. As expected, the optical appearance and homogeneity of the composite prepared by hand lay-up using the EP-Ar_3PO matrix were inferior to the other composites.

The mechanical properties were comparatively evaluated for those composites which showed the best, an intermediate and the worst fire and flammability performance. The results of their mechanical properties were also compared to those of the EPC-DDS composite.

Failure under cyclic loading is unavoidable in actual composites and is one of the most common life-limiting damages of a reinforced material, followed by delamination. The delamination of a fibre-reinforced composite is dependent on both the crack opening tensile stresses and the in-plane shear stresses. Moreover, a combination of both stresses may also be present in actual applications. As such, the effect of the different phosphorus-containing hardeners must be evaluated carefully in order to determine the delamination resistance of the composites and to assess the potential use of such phosphorus-containing matrices for demanding applications. For this reason, crack propagation experiments were carried out in mode I (tension) and mode II (shear).

An interesting correlation between the delamination resistance in either mode I or mode II and the resulting composite flame retardancy are presented in Fig. 9. The critical strain energy release rate at crack initiation in either mode was improved for all phosphorus-containing matrices. Particularly for the EPC-$ArPO_3$ and EPC-Ar_3PO composites, a simultaneous improvement in flame retardancy and delamination resistance was observed as compared to EPC-DDS. The relatively larger delamination resistance of the composites manufactured with the phosphorus-containing matrices can be ascribed to the ability of the modified thermosets to undergo

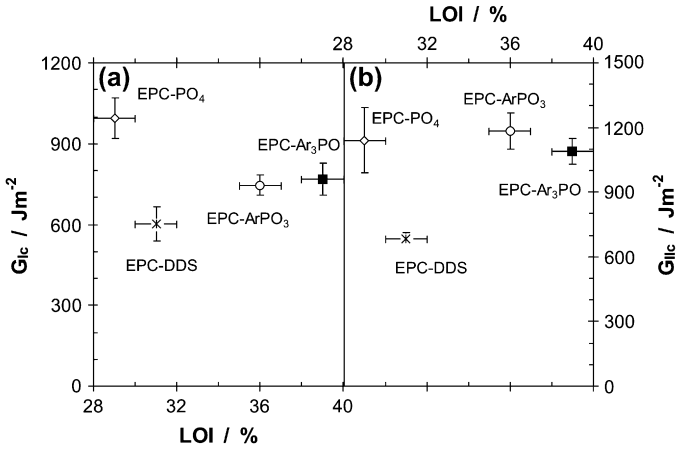

Fig. 9. Delamination resistance of the composites as a function of the LOI: (a) crack initiation values in mode I and (b) crack initiation values in mode II.

greater plastic deformation at the crack tip [41]. This observation is directly related to the average molecular weight between cross-links of the epoxy matrix, which was estimated using a statistical approach [42] to be in the order: EP-PO_4 > EP-$ArPO_3$ > EP-Ar_3PO > EP-DDS. The correlation between the delamination resistance of the phosphorus-containing composites in mode II and the average molecular weight between cross-links of the associated matrix appears to be less strong. Other factors such as matrix–fibre adhesion and the relative quality of the composite may also contribute to the observed G_{IIc} values. In summary, the matrices containing phosphorus are more capable of suppressing crack initiation in these composites than the EP-DDS matrix.

It is well known that the flexural properties and the interlaminar shear strength for UD composites are governed by the quality of the fibre–matrix adhesion [43,44] if the applied stresses act parallel to the direction of the fibres. However, for the woven fabric composites studied here, both the resulting flexural properties and interlaminar shear strength are determined by a combination of the properties of the epoxy matrix and by the quality of the fibre–matrix adhesion. Table 6 summarises the flexural properties and apparent interlaminar shear strength of the different manufactured composites. It can be seen from the data that, within experimental error of the measurement, the flexural properties and interlaminar bonding strength of the phosphorus-containing composites were not degraded as compared to the EPC-DDS composite. On the other hand, the comparatively lower values observed for EPC-Ar_3PO are a direct consequence of the quality of the resulting composite. A relatively higher amount of fabrication defects (such as microscopic cracks, voiding and poor fibre wetting) are assumed to have influenced the final mechanical performance of this particular composite negatively, given that it was prepared employing the hand lay-up technique.

Table 6
Flexural and interlaminar shear properties of the carbon fibre-reinforced composites

Composite	Flexural properties		ILSS (MPa)
	Modulus (GPa)	Strength (MPa)	
EPC-DDS	63 ± 4	940 ± 80	69 ± 5
EPC-Ar_3PO	43 ± 2	695 ± 69	55 ± 6
EPC-$ArPO_3$	60 ± 8	–	69 ± 3
EPC-PO_4	62 ± 3	1005 ± 50	71 ± 2

4. Conclusion

The pyrolysis of neat epoxy resins containing phosphine oxide, phosphinate, phosphonate, and phosphate (phosphorus contents around 2.6 wt.%) and the fire behaviour of their carbon fibre composites were studied in order to investigate the influence of the oxidation state of the phosphorus on the fire retardancy of such materials. Models for the main decomposition pathways are proposed based on a comprehensive characterisation of the thermal behaviour (TG, kinetics) and the volatile and non-volatile decomposition products (TG-FTIR, FTIR-ATR and XPS). The flammability of the composites was investigated with LOI and UL 94 tests and the fire behaviour for forced-flaming conditions with a cone calorimeter used with different irradiations. The flame retardancy mechanisms were discussed for the gas and condensed phases. The results obtained for the modified epoxy resins were compared to non-fire-retarded epoxy resins cured with DDS as hardener. It turned out that this comparison is not perfectly systematic as in particular the $-SO_2-$ group increases the intrinsic fire retardancy of the polymeric structure in the fire performance. However, the DDS–DGEBA system works as an interesting reference value for an established system.

The pyrolysis zone during a fire with its characteristic pyrolysis temperature, activation energy, char yield, release rate, and heat of combustion of the volatile pyrolysis products controls the fire behaviour of a polymeric material. Furthermore, often more than a single decomposition process or step influences the pyrolysis of a polymeric material and indeed, switching away from a main single-step decomposition is a successful flame retardancy strategy. Phosphorus-containing flame retardants are able to show a variety of flame retardancy mechanisms. They can influence several of the pyrolysis parameters, and so it is in this study. Significant interactions between the epoxy structure and the groups containing phosphorus were observed to clearly alter the decomposition pathway. The major results obtained from this study by using systematically varied phosphorus-containing hardeners can be summarised as follows:

- Volatiles containing phosphorus are released into the flame zone, resulting in flame inhibition (the heat of combustion of the volatiles is reduced by decreasing the product of combustion efficiency multiplied by the effective heat of combustion of the volatiles). The effect is the strongest for phosphine oxide, decreases with increasing oxidation and vanishes for phosphate.
- Phosphorus-containing groups influence the decomposition of the epoxy resin, resulting in a clear multi-step decomposition with mass losses between around 15 and 20 wt.% in subsequent processes after the main

decomposition step. The mass loss of the main decomposition step is reduced.

- Phosphorus-containing acids are formed and enhance the charring in the condensed phase. Apart from carbon-based char, P_xO_y and $P_xN_yO_z$ were proved in the high-temperature residue. The charring effect is the strongest for phosphate, decreases with decreasing oxidation state and becomes of minor importance for phosphine oxide.
- Phosphorus-phenoxy groups resulted in a decreased decomposition temperature, enhanced water elimination, and reduced mass loss during the main decomposition step.

The fire behaviour of the corresponding carbon fibre (60 vol.%) epoxy resin composites is influenced by the condensed and the gas phase mechanisms, but the flame inhibition in the gas phase mechanism plays the more important role. It is concluded that this result may be typical for composite structures, in which the high carbon fibre content crucially decreases the relative charring impact. Hence, the composite containing phosphine oxide shows the superior performance in terms of flammability (UL 94 and LOI) and fire behaviour (cone calorimeter).

Apart from EPC-Ar_3PO, none of the matrices containing phosphorus utilised to fabricate the composites had detrimental effects on the delamination resistance, the flexural properties or the interfacial bonding strength of the resulting part. Moreover, in some of the composites studied a simultaneous improvement in flame retardancy and mechanical performance was observed, accompanied by an adequate processability using the liquid composite moulding techniques. This observation, in turn, is what ultimately will define the potential use of such phosphorus-containing matrices for demanding applications such as in the mass transport industry.

Thus this paper presents a valuable contribution towards a directed design of new flame-retarded, fibre-reinforced composites for demanding future applications.

Acknowledgments

The authors thank the German Science Foundation (DFG) for financial support (SCHA 730/6-1, AL474/3-1, AL474/4-2; PO 575/8-1, and DO 453/4-2). Thanks also to R.-D. Schulze, J. Falkenhagen and G. Hidde for their support related to the XPS and FTIR measurements.

References

[1] Lu SY, Hamerton I. Prog Polym Sci 2002;27(8):1661–712.
[2] Levchik SV, Weil ED. Polym Int 2004;53(12):1901–29.
[3] Levchik S, Piotrowski A, Weil E, Yao Q. Polym Degrad Stab 2005; 88(1):57–62.
[4] Hergenrother PM, Thompson CM, Smith JG, Connell JW, Hinkley JA, Lyon RE, et al. Polymer 2005;46(14):5012–24.
[5] Lewin M, Weil ED. Mechanism and modes of action in flame retardancy of polymers. In: Horrocks AR, Price D, editors. Fire retardant materials. Cambridge: Woodhead Publishing; 2001. p. 31–68.
[6] Hastie JW. J Res Nat Bur Stand Sect A Phys Chem 1973;77:733–54.
[7] Schartel B, Kunze R, Neubert D. J Appl Polym Sci 2002;83(10): 2060–71.
[8] Braun U, Schartel B. Macromol Chem Phys 2004;205(16):2185–96.
[9] Davis J, Huggard M. J Vinyl Additive Technol 1996;2(1):69–75.
[10] Braun U, Schartel B. J Fire Sci 2005;23(1):5–30.
[11] Schartel B, Braun U. Polym Mater Sci Eng 2004;91:152–3.
[12] Liu YL, Hsiue GH, Lee RH, Chiu YS. J Appl Polym Sci 1997;63: 895–901.
[13] Perez RM, Sandler JKW, Altstädt V, Hoffmann T, Pospiech D, Artner J, et al. submitted for publication.
[14] Friedman HL. J Polym Sci Part C 1964;6:183–95.
[15] Stevanovic D, Jar PYB, Kalyanasundaram S, Lowe A. Compos Sci Technol 2000;60:1879–87.
[16] Chou I, Kimpara I, Kageyama K, Ohsawa I. Mode I and mode II fracture toughness measured between differently oriented plies in graphite/epoxy composites. In: Martin RH, editor. Composite materials: fatigue and fracture, vol. 5. Philadelphia: American Society for Testing and Materials; 1995. p. 132–51.
[17] Liu YL, Hsiue GH, Lan CW, Chiu YS. Polym Degrad Stab 1997;56: 291–9.
[18] Wang CS, Lin CH. J Appl Polym Sci 1999;74:1635–45.
[19] Braun U, Knoll U, Schartel B, Hoffmann T, Pospiech D, Artner J, et al. Macromol Chem Phys 2006;207:1501–14.
[20] Chin WK, Shau MD, Tsai WC. J Polym Sci Part A Polym Chem 1995;33:373–9.
[21] Shau MD, Wang TS. J Polym Sci Part A Polym Chem 1996;34:387–96.
[22] Levchik SV, Camino G, Luda MP, Costa L, Muller G, Costes B. Polym Degrad Stab 1998;60:169–83.
[23] Derouet D, Morvan F, Brosse JC. J Appl Polym Sci 1996;62:1855–68.
[24] Wang CS, Shieh JY. Eur Polym J 2000;36:443–52.
[25] Lin JF, Ho CF, Huang SK. Polym Degrad Stab 2000;67:137–47.
[26] Wang Q, Shi W. Polym Degrad Stab 2006;91:1747–54.
[27] Liu W, Varley RJ, Simon GP. Polym Degrad Stab 2006;47:2091–8.
[28] Dyakonov T, Mann PJ, Chen Y, Stevenson WTK. Polym Degrad Stab 1996;54:67–83.
[29] Balabanovich AI, Hornung A, Merz D, Seifert H. Polym Degrad Stab 2004;85:713–23.
[30] Thomas LC. Interpretation of the IR spectra of organophosphorus compounds. London: Heyden; 1974.
[31] Li X, Ou Y, Shi Y. Polym Degrad Stab 2002;77:383–90.
[32] Deng J, Shi W. Eur Polym J 2004;40:1137–43.
[33] Hsiue GH, Liu YL, Tsiao J. J Appl Polym Sci 2000;78:1.
[34] Varma IK, Gupta U. J Macromol Sci Chem 1986;A23:19–36.
[35] Levchik SV, Camino G, Costa L, Luda MP. Polym Degrad Stab 1996;54: 317–22.
[36] Schartel B, Pötschke P, Knoll U, Abdel-Goad M. Eur Polym J 2005; 41:1061–70.
[37] Schartel B, Braun U. e-Polymers 2003; art. no. 013.
[38] Zhu S, Shi W. Polym Degrad Stab 2003;82:435–9.
[39] Duquesne S, Lefebvre J, Seeley G, Camino G, Delobel R, Le Bras M. Polym Degrad Stab 2004;85:883–92.
[40] Price D, Bullett KJ, Cunliffe LK, Hull TR, Milnes GJ, Ebdon JR, et al. Polym Degrad Stab 2005;88:74–9.
[41] LeMay JD, Kelley FN. Adv Polym Sci 1986;78:115–48.
[42] Vallo CI, Frontini PM, Williams RJJ. J Polym Sci Part B Polym Phys 1991;29:1503–11.
[43] Kim JK, Mai YW. Engineered interfaces in fiber reinforced composites. New York: Elsevier; 1998. p. 191–96, 329–65.
[44] Barbero EJ. Introduction to composite materials design. Philadelphia: Taylor & Francis; 1999. p. 21, 97–9.